

Electromagnetic propagation in nanostructures

Michael A. Mastro^a, R. T. Holm^a, Charles R. Eddy Jr.^a and Jihyun Kim^{b,*}

^aU.S. Naval Research Laboratory, Electronics Science & Technology Division, 4555 Overlook Ave., SW, Washington, D.C. 20375, U.S.A.

^bDepartment of Chemical and Biological Engineering, Sungbuk-Gu, Anam-Dong 5-1, Korea University, Seoul, Korea

Future integrated circuit technology will feature a fusion of optical and optoelectronic components with traditional electronic devices. Information can be rapidly transmitted as light in dielectric waveguides, photonic crystal guides and metallic nanoarrays. This paper presents a description of electromagnetic propagation in semiconductor and metallic nanostructures. Diffraction effects will dominate the propagation of light when the dimension of the cavity or device approaches its wavelength. The plasmonic effect circumvents this problem by propagating the light wave through highly localized conduction electrons in a noble metal [1].

Key words: Metallic Nanostructure, Optoelectronics

Introduction

Three technologies to propagate light on a semiconductor chip, in increasing levels of complexity, are dielectric waveguides, photonic crystals, and metallic plasmonic structures [2]. Confinement in dielectric waveguides and photonic crystals is on the order of the wavelength of the propagated light wave. The simple miniaturization of optics and optoelectronics to the nano-scale introduces adverse optical effects when the size is comparable to or less than the wavelength of light generated [3]. To circumvent this effect, light can be propagated at the intra-transistor level along plasmonic waveguides. The small size of these features necessitates an understanding of electromagnetic wave propagation in nanostructures.

Cavity Design

For certain waveguide constructions, wave propagation can not be represented by a simple transverse electric (TE) or transverse magnetic (TM) mode. In restricted dielectric cavities, such as a fiber optic waveguide or a GaN nano-wire resonant cavity, field configurations arise that are a combination of TE and TM modes. These mixed hybrid modes are termed hybrid electric (HE_{nm}) or magnetic (EH_{nm}) to indicate that the mixed electromagnetic field is more analogous to a corresponding TE(H) or TM(E) mode. The subscript index n designates the angular symmetry and m designates the radial field dependence. These hybrid modes are also assigned the moniker of a hybrid electromagnetic (HEM) mode although

there are inconsistencies in the literature regarding this classification [4].

In general, only a restricted number of unattenuated waveguide modes will concentrate their propagating waves within a finite cylindrical dielectric waveguide. Simple TE(H) and TM(E) modes are symmetric and do not display angular variations. When the dielectric cylinder diameter is on the order of the propagating wavelength, then non-symmetric hybrid modes propagate.

Based on waveguide diameter, TE, TM and certain hybrid modes exhibit cutoff frequencies, below which the propagating wave will be rapidly damped (or simply not exist). Conversely, the fundamental HE₁₁ mode has a cutoff frequency of zero (or approximately zero) and thus can propagate unattenuated in waveguides thinner than the wavelength, such as in a GaN nano-wire. Following Balanis [4], the hybrid modes internal to a dielectric rod can be written as:

$$H_{\phi}^d = \frac{-j}{(\beta_p^d)} [m\beta_z A_m J_m + \omega \epsilon_d (\rho \beta_p^d) B_m J_m] \cos(m\phi) e^{-jB_z z} \quad (1)$$

$$H_{\rho}^d = \frac{-j}{(\beta_p^d)} [\beta_z (\rho \beta_p^d) A_m J_m + m \omega \epsilon_d B_m J_m] \sin(m\phi) e^{-jB_z z} \quad (2)$$

$$H_z^d = A_m J_m (\rho \beta_p^d) \sin(m\phi) e^{-jB_z z} \quad (3)$$

$$E_{\phi}^d = \frac{-j}{(\beta_p^d)} [\omega \mu_d A_m J_m (\rho \beta_p^d) + m \beta_z B_m c] \sin(m\phi) e^{-jB_z z} \quad (4)$$

$$E_{\rho}^d = \frac{-j}{(\beta_p^d)} [m \omega \mu_d A_m + \beta_z (\rho \beta_p^d) B_m J_m] \sin(m\phi) e^{-jB_z z} \quad (5)$$

$$E_z^d = B_m J_m (\beta_p^d \rho) \cos(m\phi) e^{-jB_z z} \quad (6)$$

*Corresponding author:

Tel : +82-2-3290-3291

Fax: +82-2-926-6102

E-mail: jhkim@prosys.korea.ac.kr

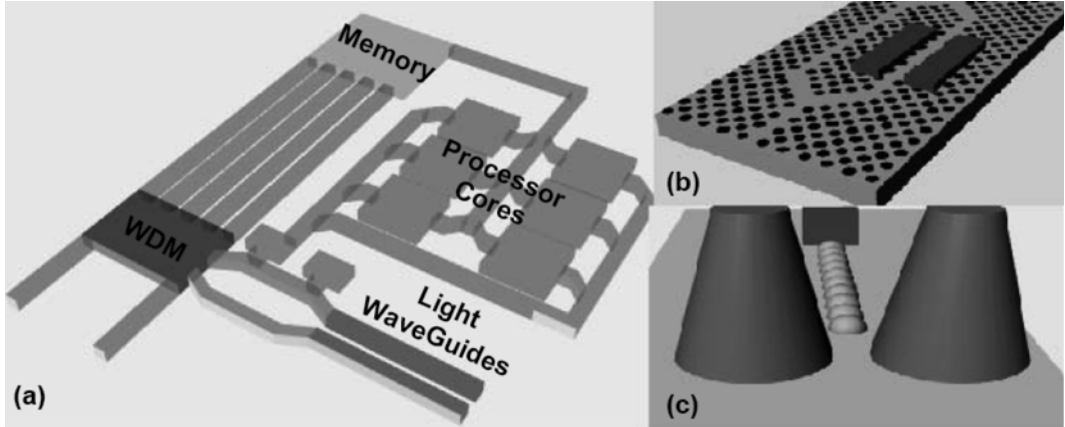


Fig. 1. Schematic of next-generation processor device merging traditional electronic CMOS technology with optic based technology including (a) dielectric waveguides (b) micrometer-scale photonic crystal propagation and switching technology such as a Mach-Zender Interference Modulator as well as (c) plasmonic based emitters/detectors coupled to noble metal arrays as a nano-scale confined propagation channel.

with

$$(\beta_p^d)^2 + \beta_z^2 = \beta_d^2 = \omega^2 \mu_0 \epsilon_0 \mu_r \epsilon_r \rightarrow k_0^2 = \omega^2 \mu_0 \epsilon_0 \quad (7)$$

where r , the radial distance is less than a , the radius of the dielectric, z is the axial distance, ϕ is the angle relative to an arbitrary x -axis, ϵ_0 and ϵ_r are the vacuum and relative permittivity, μ_0 and μ_r are the vacuum and relative magnetic permeability, $\beta_{p,z,d}$ are the propagation constants which are related to $k_{p,z,d}$, the effective wave vector in the dielectric, k_0 ($= \omega_0/c$) is the wave vector in vacuum, and ω_0 , is the angular frequency [4].

Application of boundary conditions that match the E and H fields at the dielectric surface [4] yields an eigenvalue equation in terms of the appropriate constants-including A_m and B_m -that is used to calculate the supported modes in the dielectric rod. A similar set of equations can be developed for the field that extends outside the rod ($\rho \geq a$).

In all cases, $k_0 < \beta_z < k_0 \epsilon_r$, where the phase velocity, β_z , approaches $k_0 \epsilon_r$ at zero or cutoff frequency, and

approaches the wave vector in vacuum at high frequency. If β_z surpasses $k_0 \epsilon_r$ then mathematically an imaginary component enters the field equations. Physically, this implies an evanescent decay along the cylinder z -axis. These boundary conditions and equations are matched to the evanescent wave exterior to the cavity with an analogous set of equations and constants. The Bessel and modified Bessel functions define the family of waves that are supported in the cylindrical dielectric as described by the characteristic wave equations. That is, the Bessel function defines the cut-off wavelength above which the mode can propagate as $2\pi a/\lambda \geq 2.405$ (TE_{01} , TM_{01}), 3.83 (HE_{12} , EH_{11}), 5.136 (TE_{02}, TM_{02}), etc., except for the HE_{11} mode which does not have a cut-off [4].

Propagation of a wave-packet through a guide is described as a linear combination of waveguide modes, where a dispersion relation (Fig. 2.) exists for each mode between the propagation constant, β_z , and the frequency, ω [5]. For extremely narrow dielectric rods (or wires), only the fundamental hybrid HE_{11} mode is supported. A significant fraction of the HE_{11} field is external to the bare dielectric core, thus hampering the Q value of resonant cavity [6]. At larger diameters but still less than the vacuum wavelength, other modes can be supported, particularly the TE_{01} and TM_{01} mode. There is a general trend of increased confinement with increasing rod diameter or increasing wavevector, k (~frequency), for all modes. If present, the TE_{01} and TM_{01} modes have superior axial confinement and thus may dominate over a loosely bound hybrid mode in a resonant cavity such as in a III-nitride nano-wire [7, 8].

The analytical expressions for the electric field, E , and magnetic field, H , patterns inside a dielectric rod are imaged in Fig. 3 [4, 9]. The reader is directed to the fundamental original development in Okoshi [9] and Balanis. [4] The rectangular cross-sections that bisect the cylinder show the symmetry between the TE and TM modes for a rod length one-half the optical wavelength.

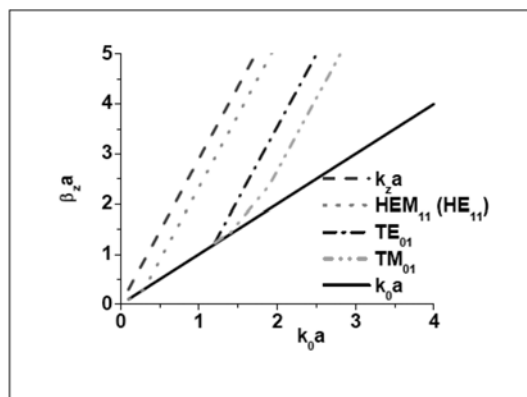


Fig. 2. (Color Online) Guided mode dispersion curves at 3.35 eV for a GaN ($\epsilon_r = 8.4$) nano-rod. The k_z and k_0 wave vectors denote the light line in the dielectric and vacuum, respectively.

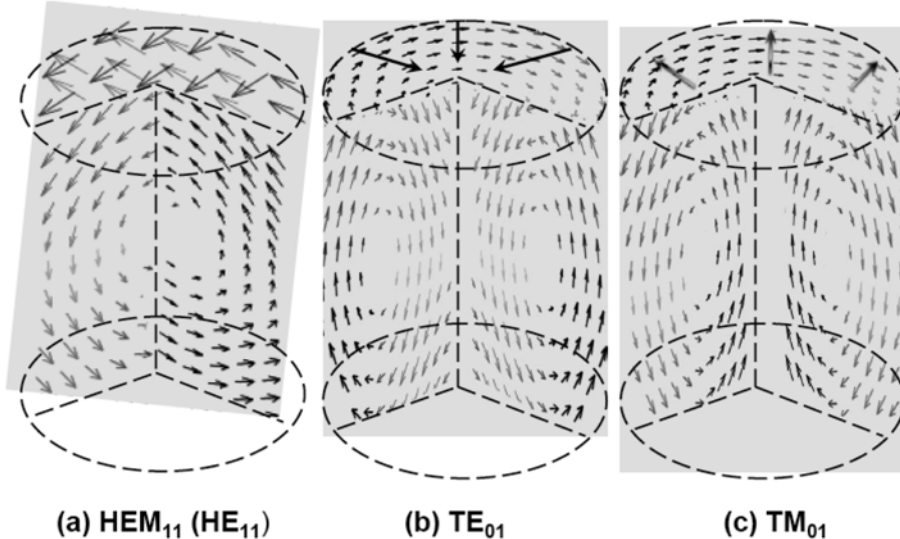


Fig. 3. Calculation and visualization of the supported modes for a dielectric rod (Color Online) E (grey print; light blue, green, red online) and H (black) field patterns of (a) HEM₁₁, (b) TE₀₁, and (c) TM₀₁ modes [4, 9].

Historically, TM₀₁ is referred to as circular-magnetic (or radial-electric) and TE₀₁ is designated as circular-electric (or radial-magnetic) [10-17], which fittingly describes the wave patterns displayed in Fig. 3.

Plasmonic Enhancement

Electromagnetic excitation of a continuous metal-dielectric interface creates charge density waves on the surface with free electrons propagating along the interface of this conductor and a dielectric medium.¹⁸ The wave character of this surface plasmon polariton (SPP) field decays exponentially perpendicular to the metal and dielectric interface [19]. Thus, the field at the free surface of the metal is increased and perpendicularly confined. A metallic stripe is used to provide micrometer-scale lateral localization of the SPP. The SPP can propagate over several micrometers; however, this is diminished with sub- micrometer localization [20]. The wavevector, k , of a SPP mode of coherent longitudinal charge oscillations of the conduction electrons is given by [21-24]:

$$k = \frac{\omega}{c} \sqrt{\frac{\epsilon_{\text{metal}} \epsilon_{\text{dielectric}}}{\epsilon_{\text{metal}} + \epsilon_{\text{dielectric}}}} \quad (8)$$

An alternative waveguide is an ordered array of nano-particles on a continuous dielectric film for finer lateral confinement of light compared to the traditional diffraction limit. The light propagates to near micrometer lengths with nano-scale lateral confinement via near-field particle interactions.

When a light-wave interacts with a metal, the electrons respond resistively with a velocity proportional to the electric field. At low frequency, the metal conduction electrons lose the energy of the field via collisions with ions in the metal which creates phonons (heat). At high

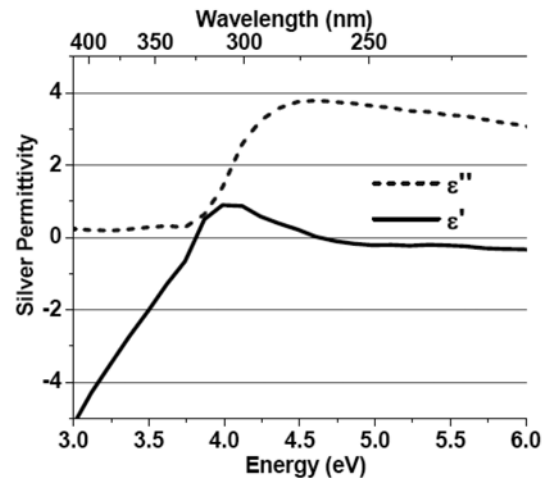


Fig. 4. Dielectric function of bulk silver for real, ϵ' (solid line) and imaginary, ϵ'' (dotted line) permittivity, $\epsilon = \epsilon' + i\epsilon''$ [11]. Note that III-nitride optoelectronic emission and nano-scale silver resonance can be readily tailored to access this frequency range.

frequency, the mean time for collision is reduced and thus the electrons travel freely, proportional to the oscillating electric field. This system can be described as a simple Drude metal with a dielectric constant, $\epsilon = 1 - \omega_p^2/\omega^2$. The plasma frequency of a metal, $\omega_p^2 = ne^2/m_e\epsilon_0$ is the transition point from a reflecting (negative dielectric constant) at low frequency light to transparency (positive dielectric constant) at high- frequency light. Gold, copper and silver are of interest as their electron gas plasma frequencies exist at or near visible frequencies and, particularly in the case of silver (Fig. 4), strongly interact with visible and ultra-violet light-waves.

Electromagnetic excitation creates a non-dispersive, localized surface plasmon (LSP) in nano-scale metal particles [12]. The conduction electrons in the particle will oscillate as a dipole with a plasmon resonance

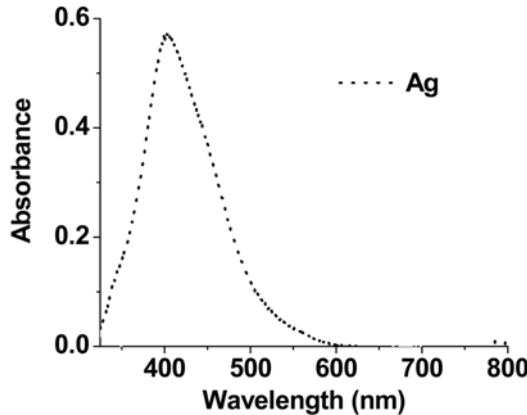


Fig. 5. Ultra-violet/white light absorbance spectra of silver nano-particles on a silicon substrate. The peak at 407 nm corresponds to the plasmonic response of silver nano-particles.

[13, 14]. This induced homogeneous polarization inside the metal can be expressed as the dipole polarization, $\alpha = 4\pi a^3(\epsilon_{\text{metal}} - \epsilon_{\text{dielectric}})/(\epsilon_{\text{metal}} + 2\epsilon_{\text{dielectric}})$ when the particle size is sub-wavelength ($a < < \lambda$). Thus, when $\epsilon_{\text{metal}} \approx 2$, the polarization is resonantly enhanced at the Frohlick frequency, i.e., LSP frequency [15]. In larger particles (> 100 nm) the plasmon resonance red-shifts from retardation effects that prevent electrons from moving in phase as this interaction can only travel at a certain speed (less than the velocity of light) [16].

A related expression describes the polarization of an elliptical particle, with dimensions of a , b , and c by, $\alpha = 4/3\pi abc(\epsilon_{\text{metal}} - \epsilon_{\text{dielectric}})/(\epsilon_{\text{metal}} - L_i(\epsilon_{\text{metal}} - \epsilon_{\text{dielectric}}))$ where, L_i is the normalized geometric portion and sums to unity.¹⁷ At a specific excitation, a dielectric rod will show a short-wavelength peak for polarization perpendicular to the long major axis and a long-wavelength peak for polarization parallel to the long major axis.

To illustrate these effects, silver nanoparticles were fabricated and dispersed on a silicon substrate (Fig. 5). The silver deposition was conducted in a Parr pressure-restricted solvothermal chamber. The solvent consisted of 10 ml of methanol, ethylene glycol, hexane, or glycerin mixed with 400 mg sodium hydroxide and 250 mg silver nitrate in a fitted Teflon cup. The Teflon cup was loaded into the sealed Parr bomb which was subsequently placed for one hour in an oven operating at 180°C. The *ex situ* reflectance was measured at normal incidence using a halogen lamp as a source and reflected beam was dispersed through an Ocean Optics S2000 spectrometer with a 50 μm slit.

A number of elegant solutions have been developed since the pioneering work of Mie made calculations of scattering by an isolated metal particle [25-27]. Nevertheless, even simple geometric alteration of a nano-scale metal structure or its environment will alter the electromagnetic resonance beyond what can be described by an analytical

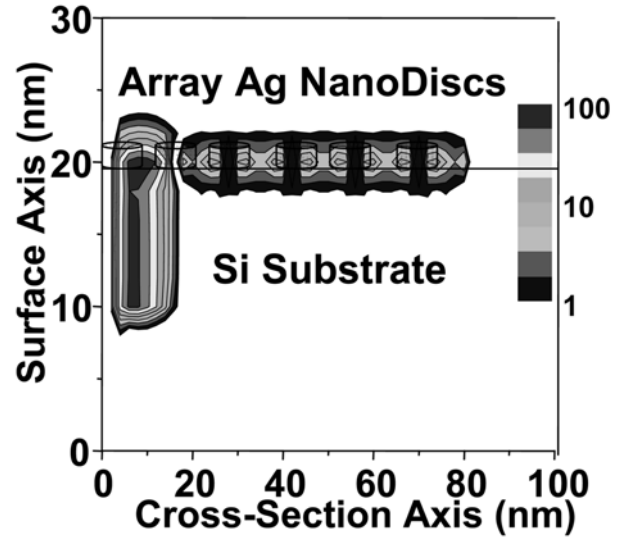


Fig. 6. Plasmon wave (left to right) propagation along a array of silver nanodiscs placed on the surface of a silicon substrate.

expression.

To describe electromagnetic propagation in an array of silver nanoparticles as pictured in Fig. 1(c), it is necessary to employ a three-dimensional finite difference time domain (FDTD) computational electrodynamics modeling technique. Maxwell's equations were modified to central-difference equations, discretized, and implemented in object-oriented C++ code. The electric and magnetic fields are solved in an alternating leapfrog scheme originally developed by Yee [28]. A perfectly matched layer (boundary condition) was employed to diminish outer-boundary reflection errors [29].

In the simulation, an electromagnetic wave was input at the leading edge of a one-dimensional array of silver nanoparticles placed on the surface of a Si substrate. This plasmon wave propagates by the successive interaction of particles along the array. This array is a highly confined optical waveguide with minimal loss into the Si substrate.

Conclusions

The integration of optical components with electronic components present a number of engineering and scientific problems [30-33]. Simple dielectric waveguides are a relatively simple structure to fabricate, however, actual ultra large scale integration is difficult due to the inherent size differential with electronic transistors [34-38]. Nevertheless, dielectric waveguides are well-suited for long-run interconnects in a multi-core die. Plasmonic based transfer along noble metal nanoparticles is promising but the propagation length is limited by the inherent absorption. Commercial implementation of one or a

mixture of the optical components presented in this work is conceivable [40-43].

Acknowledgements

Research at the Naval Research Lab was supported by Office of Naval Research. Research at Korea University was supported by BK21 Program.

References

1. E. Ozbay, Science 331, 189-193 (2006).
2. M. A. Mastro, J. A. Freitas, Jr., O. Glembocki, C. R. Eddy, Jr., R. T. Holm, R. L. Henry, J. Caldwell, R.W. Rendell, F. Kub, J-H. Kim, Nanotechnology, 18, 265401 (2007).
3. M. A. Mastro, R.T. Holm, N. D. Bassim, C. R. Eddy, Jr., R. L. Henry, M. E. Twigg, A. Rosenberg, Jpn. J. Appl. Phys. 45, L814-L816 (2006).
4. C. A. Balanis, Advanced Engineering Electromagnetics. New York, Wiley (1989).
5. A. A. Govyadinov, V. A. Podoskiy, Phys. Rev. Lett., 97, 223902(4pages) (2006).
6. A. V. Maslov, C. Z. Ning, J. Appl. Phys. 99, 024314 (10pages) (2006).
7. A. V. Maslov, C. Z. Ning, Opt. Lett. 29, 572-574 (2004).
8. A. V. Maslov, C. Z. Ning, IEEE. J. Quantum Electron. 40, 1389-1397. (2004).
9. T. Okoshi, Optical Fibers, Academic Press (1982).
10. G. C. Southworth, Principles and Applications of Waveguide Transmission, D. Van Mostrand Company (1950).
11. P. B. Johnson, R. W. Christy, Phys. Rev. B 6, 4370-4379 (1972).
12. J. Kottmann, O. Martin, D. Smith, S. Schultz, Optics Express 6, 213-219 (2000).
13. U. Kreibig, M. Vollmer "Optical Properties of Metal Clusters", Springer, Berlin (1995).
14. J. Kottmann O. Martin, Opt. Express 8, 655-663 (2001).
15. S. A. Maier, H. A. Atwater, J. Appl. Phys. 98, 011101 (10pages) (2005).
16. J. Lee, T. Javed, T. Skeini, A. O. Govorov, G. W. Bryant, N. A. Kotov, Angewandte Chemie 45, 4819-4823 (2006); M. Meier, A. Wokaun, Opt. Let. 8, 581-583 (1983).
17. S. Link, M. A. El-Sayed, Int. Rev. Phys. Chem. 19, 409-453 (2000).
18. G. Leveque, O. J. F. Martin, Optics Exp. 14 9971-9981 (2006).
19. S. Wedge, W. L. Barnes, Opt Expr. 12, 3673-3685 (2004).
20. C. F. Bohren, D. R. Huffman, Absorption and Scattering of Light by Small Particles, Wiley, New York (1983).
21. H. Raether, Surface Plasmons on Smooth and Rough Surfaces and on gratings, Springer, Berlin (1988).
22. G. B. Airy, Transactions of the Cambridge Philosophical Society 5, 283-291 (1835).
23. A. Graff, D. Wagner, H. Diltbacher U. Kreibig, European Physical Journal D 34, 263-269 (2005).
24. E. N. Economou, Physical Review 182, 539-554 (1969).
25. G Mie, "Beiträge zur Optik trüber Medien, speziell kolloidaler Metallösungen", Leipzig, Ann. Phys. 25, 377-445 (1908).
26. A. Stratton: Electromagnetic Theory, New York: McGraw-Hill (1941).
27. H. C. van de Hulst: Light scattering by small particles, New York, Dover (1981).
28. K. Yee, IEEE Transactions on Antennas and Propagation 14, 302-307 (1966).
29. J. Berenger, J. of Comp. Phys. 114, 185-200 (1994).
30. C. Kittel, Introduction to Solid State Physics, Wiley, New York (1996).
31. H. Raether, Surface Plasmons, vol. 111 of Springer-Verlag Tracts in Modern Physics, Springer-Verlag, New York, (1988).
32. M. A. Mastro, M. Fatemi, D. K. Gaskill, K-K Lew, B. L. Van Mil, C. R. Eddy Jr., C. E. C. Wood, J. Appl. Phys., 100, 093510(5pages) (2006).
33. M. A. Mastro, C. R. Eddy Jr., D. K. Gaskill, N. D. Bassim, J. Casey, A. Rosenberg, R. T. Holm, R. L. Henry, M. E. Twigg, J. Crystal Growth, 287, 610-614 (2006).
34. H. Xu, J. Aizpurua, M. Kaell, P. Apell, Phys. Rev. E 62, 4318-4324 (2000).
35. M. A. Mastro, N. D. Bassim, J. Freitas, M. E. Twigg, C. R. Eddy, Jr., D.K. Gaskill, R. L. Henry, R. T. Holm, J. Kim, P. G. Neudeck, A. J. Trunek, J. A. Powell, J. Cer. Proc. Res. (in press).
36. S. Link, M.A. El-Sayed, J. Phys Chem. B 103, 8410-8426 (1999); J. Aizpurua, Garnett W. Bryant, Lee J. Richter, F. J. García de Abajo, Brian K. Kelley, T. Mallouk, Phys. Rev. B. 71, 235420(9pages) (2005); J. Aizpurua, P. Hanarp, D. S. Sutherland, M. Kall, G. W. Bryant, F. J. G. de Abajo, Phys. Rev. Lett. 90, 057401(4pages) (2003).
37. K. Okamoto, S. Vyawahare, A. Scherer, J. Op. Soc. Am. B 23, 1674-1678 (2006).
38. E. Purcell, Phys. Rev. 69, 37-38 (1946).
39. A. Neogi, Henry O Everitt, H. Morkoç, T. Kuroda, A. Tackeuchi, IEEE Trans. on Nanotech. 2, 10-14 (2003).
40. M. A. Mastro, R. T. Holm, N. D. Bassim, C. R. Eddy, Jr., D. K. Gaskill, R. L. Henry, M. E. Twigg, Appl. Phys. Lett. 87, 241103(3pages) (2005).
41. M. A. Mastro, R. T. Holm, N. D. Bassim, D. K. Gaskill, J. C. Culbertson, M. Fatemi, C. R. Eddy, Jr., R. L. Henry M. E. Twigg: J. Vac. Sci. Technol. A 24, 1631-1634 (2006).
42. A. Neogi, H. Morkoç, Nanotechnology 15, 1252-1255 (2004).
43. M. A. Mastro, J. A. Freitas, R. T. Holm, C. R. Eddy, Jr., J. Caldwell, K. Liu, O. Glembocki, R. L. Henry, J-H. Kim, Appl. Surf. Chem. 253-14, 6157-6161 (2007).